

Published in final edited form as:

*J Nucl Med.* 2012 February ; 53(2): 287–294. doi:10.2967/jnumed.111.095653.

## Quantitative preclinical imaging of TSPO expression in glioma using *N,N*-diethyl-2-(2-(4-(2-(<sup>18</sup>F)-fluoroethoxy)phenyl)-5,7-dimethylpyrazolo[1,5-*a*]pyrimidin-3-yl)acetamide

Dewei Tang<sup>1,2</sup>, Matthew R. Hight<sup>1,3</sup>, Eliot T. McKinley<sup>1,4</sup>, Allie Fu<sup>1</sup>, Jason R. Buck<sup>1,5</sup>, R. Adam Smith<sup>1,5</sup>, Mohammed Noor Tantawy<sup>1,5</sup>, Todd E. Peterson<sup>1,2,5,6</sup>, Daniel Colvin<sup>1,5</sup>, M. Sib Ansari<sup>1,5</sup>, Mike Nickels<sup>1,5</sup>, and H. Charles Manning<sup>1,2,4,5,7,8</sup>

<sup>1</sup>Vanderbilt University Institute of Imaging Science, Vanderbilt University Medical Center, Nashville, Tennessee 37232

<sup>2</sup>Program in Chemical and Physical Biology, Vanderbilt University Medical Center, Nashville, Tennessee 37232

<sup>3</sup>Interdisciplinary Materials Science Program, Department of Physics & Astronomy, Vanderbilt University, Nashville, Tennessee 37232

<sup>4</sup>Department of Biomedical Engineering, Vanderbilt University, Nashville, Tennessee 37232

<sup>5</sup>Department of Radiology and Radiological Sciences, Vanderbilt University Medical Center, Nashville, Tennessee 37232

<sup>6</sup>Department of Physics & Astronomy, Vanderbilt University, Nashville, Tennessee 37232

<sup>7</sup>Department of Neurosurgery, Vanderbilt University Medical Center, Nashville, Tennessee 37232

<sup>8</sup>Vanderbilt Ingram Cancer Center, Vanderbilt University Medical Center, Nashville, Tennessee 37232

### Abstract

There is a critical need to develop and rigorously validate molecular imaging biomarkers to aid diagnosis and characterization of primary brain tumors. Elevated expression of translocator protein (TSPO) has been shown to predict disease progression and aggressive, invasive behavior in a variety of solid tumors. Thus, noninvasive molecular imaging of TSPO expression could form the basis of a novel, predictive cancer imaging biomarker. In quantitative preclinical PET studies, we evaluated a high-affinity pyrazolopyrimidinyl-based TSPO imaging ligand, *N,N*-diethyl-2-(2-(4-(2-(<sup>18</sup>F)-fluoroethoxy)phenyl)-5,7-dimethylpyrazolo[1,5-*a*]pyrimidin-3-yl)acetamide (<sup>18</sup>F]DPA-714), as a translational probe for quantification of TSPO levels in glioma.

**Methods**—Glioma-bearing rats were imaged with [<sup>18</sup>F]DPA-714 in a microPET system. Dynamic images were acquired simultaneously upon injection of [<sup>18</sup>F]DPA-714 (130 – 200 MBq/ 0.2 mL). Arterial blood was collected to derive the input function (AIF), with HPLC radiometabolite analysis performed upon select samples for AIF correction. Compartmental modeling was performed using the corrected AIF. Specific tumor cell binding of DPA-714 was evaluated by radioligand displacement of [<sup>3</sup>H]PK 11195 with DPA-714 *in vitro* and displacement

Corresponding Author: H. Charles Manning, Ph.D., Vanderbilt University Institute of Imaging Science (VUIIS), Vanderbilt University Medical School, 1161 21st Ave. S., AA 1105 MCN, Nashville, TN 37232-2310; Tel: (615) 322-3793; Fax: (615) 322-0734; henry.c.manning@vanderbilt.edu.

First Author: Dewei Tang, B.S., Graduate Student, Vanderbilt University Institute of Imaging Science (VUIIS), Vanderbilt University Medical School, 1161 21st Ave. S., AA 1105 MCN, Nashville, TN 37232-2310; Tel: (615) 322-8430; Fax: (615) 322-0734; (dewei.tang@vanderbilt.edu)

of [<sup>18</sup>F]DPA-714 with excess DPA-714 *in vivo*. Immediately following imaging, tumor and healthy brain tissues were harvested for validation by western blotting and immunohistochemistry.

**Results**—[<sup>18</sup>F]DPA-714 was found to preferentially accumulate in tumors with modest uptake in contralateral brain. Infusion with DPA-714 (10 mg/kg) displaced [<sup>18</sup>F]DPA-714 binding by greater than 60% on average. Tumor uptake of [<sup>18</sup>F]DPA-714 was similar to another high-affinity TSPO imaging ligand, [<sup>18</sup>F]PBR06, and agreed with *ex vivo* assay of TSPO protein levels in tumor and healthy brain.

**Conclusions**—These studies illustrate the feasibility of using [<sup>18</sup>F]DPA-714 for visualization of TSPO-expressing brain tumors. Importantly, [<sup>18</sup>F]DPA-714 appears suitable for quantitative assay of tumor TSPO levels *in vivo*. Given the relationship between elevated TSPO levels and poor outcome in oncology, these studies suggest the potential of [<sup>18</sup>F]DPA-714 PET to serve as a novel predictive cancer imaging modality.

### Keywords

Glioma; TSPO; Pyrazolopyrimidine; DPA-714; Positron Emission Tomography

## INTRODUCTION

Malignant gliomas are the most common primary brain tumor and are characterized by invasive growth and recalcitrance to therapy. Currently, diagnosis and grading of gliomas are based upon the pathology of resected specimens with limitations inherent to sampling errors and heterogeneity. Given these limitations, clinical decisions are routinely guided by imaging(1). The most common imaging metrics employed to detect and diagnose brain tumors are computed tomography (CT) and magnetic resonance imaging (MRI). These modalities provide little, if any, molecular information attributable to the pathological status of the disease. Furthermore, numerous studies document the inherent difficulty associated with determination of brain tumor extent using CT and/or MRI, particularly with infiltrative disease. Positron emission tomography (PET) imaging using [<sup>18</sup>F]FDG is an important technique for brain tumor detection. However, high glucose uptake in normal brain results in modest tumor-to-background ratios with [<sup>18</sup>F]FDG, which can confound delineation of disease margins and subsequent grading. Therefore, there is a considerable need to develop and validate improved molecular imaging techniques suitable for detection and/or molecular profiling of brain tumors(2).

Translocator protein (TSPO), also referred to as peripheral benzodiazepine receptor (PBR), is an 18 kDa protein typically localized to the outer mitochondrial membrane. TSPO participates in regulation of numerous cellular processes, including cholesterol metabolism, steroid biosynthesis, cellular proliferation, and apoptosis. In normal tissues, TSPO expression tends to be highest in steroid-producing and mitochondrial-enriched tissues such as skeletal muscle, renal tissue, and myocardium, while tissues such as liver and brain exhibit comparatively modest expression(3). Elevated TSPO expression is found in numerous disease states, including neuroinflammation(4) and neurological disorders such as Alzheimer's(5) and Huntington's diseases(6), as well as cancers of the breast(7, 8), prostate(9), oral cavity(10), colon(11–13), liver(14), and brain(15, 16). Elevated TSPO expression has also been linked with disease progression and diminished survival in patients with oral(10, 17), colorectal(11), breast(18), and brain(19) cancer. Additionally, elevated TSPO levels appear to be associated with aggressive, metastatic behavior in breast and colorectal cancer(7, 20). Collectively, these data illuminate TSPO expression as a potentially important prognostic biomarker in oncology and suggest the utility of tumor-selective TSPO PET ligands for cancer imaging.

Recently, a variety of novel TSPO PET ligands have emerged from the literature, including aryloxyanilides, indoleacetamides, pyrazolopyrimidines, and imidazolepyridines(21). We recently reported  $^{18}\text{F}$ -*N*-fluoroacetyl-*N*-(2,5-dimethoxybenzyl)-2-phenoxyaniline ( $^{18}\text{F}$ ]PBR06) as a high-affinity tracer for visualization of brain tumors, as well as quantification of TSPO expression in tumor and normal tissue(22). The goal of the present study was to evaluate another high-affinity TSPO PET ligand,  $^{18}\text{F}$ ]DPA-714, in cancer imaging studies. Our data illustrate the feasibility of using  $^{18}\text{F}$ ]DPA-714 for visualization of TSPO-expressing brain tumors. Importantly,  $^{18}\text{F}$ ]DPA-714 appears suitable for quantitative assay of tumor TSPO levels *in vivo*. Given the relationship between elevated TSPO levels and poor outcome in oncology, these studies suggest the potential of  $^{18}\text{F}$ ]DPA-714 PET to serve as a novel and predictive cancer imaging modality.

## MATERIALS AND METHODS

### Chemicals, Ligand and Radioligand Precursor Preparation

$^3\text{H}$ ]PK 11195 was purchased from PerkinElmer. Phosphate buffered saline (PBS) and CytoScint ES Liquid Scintillation Cocktail were purchased from MP Biomedicals. All synthesis reagents were purchased from Sigma-Aldrich.  $^{19}\text{F}$ ]DPA-714 (DPA-714) and radioligand precursor were prepared according to published methods(23).

### *In Vitro* Radioligand Binding Assay

Radioligand binding experiments were conducted utilizing C6 glioma cell lysates as previously described, using DPA-714 as the cold ligand(22, 24). All experiments were performed in triplicate.

### Radioligand Preparation

$^{18}\text{F}$ ]DPA-714 was prepared analogously to published methods(25). In short, using a commercial apparatus (TRACERlab FXF-N, GE Medical Systems), aqueous  $^{18}\text{F}$ ]fluoride ion (~ 111 GBq) was dried by iterative cycles of addition and evaporation of acetonitrile, followed by complexation with  $\text{K}^+ \cdot \text{K}^{+2.2.2} / \text{K}_2\text{CO}_3$ . The complex was reacted with 4-(3-(2-(diethylamino)-2-oxoethyl)-5,7-dimethylpyrazolo[1,5-*a*]pyrimidin-2-yl)phenethyl 4-methylbenzenesulfonate (3.0 mg) at 165°C for 5 min in dimethyl sulfoxide (0.6 mL). Purification of  $^{18}\text{F}$ ]DPA-714 was carried out using reversed-phase HPLC (C18, Dynamax 250 × 21.4 mm; Varian) eluted at 6.0 mL/min with 10 mM  $\text{NaH}_2\text{PO}_4$  buffer (pH 6.7) and ethanol (47.5:52.5; v/v).  $^{18}\text{F}$ ]DPA-714 was collected, washed with 120 mL water (deionized), and eluted from a C18 Sep-Pak with ethanol (1.0 mL) into a sterile flask loaded with saline (9.0 mL). Typical specific activities were 418 TBq/mmol.

### Rat Model

All studies involving animals were conducted in compliance with federal and institutional guidelines. Two weeks prior to imaging, healthy male Wistar rats (n=14) were stereotactically inoculated in the right hemisphere with  $1.0 \times 10^5$  C6 glioma cells (American Type Tissue Collection, ATTC). Prior to imaging, all rats were affixed with venous and arterial catheters.

### MR Imaging

MRI was used to localize C6 tumors. Rats were secured in a prone position in a 38-mm inner diameter radiofrequency coil and placed in a Varian 4.7T horizontal bore imaging system (Varian Inc.). A constant body temperature of 37 °C was maintained using heated airflow. An initial multislice gradient echo imaging sequence [repetition time (TR) = 150 ms; echo time (TE) = 3.5 ms; 128 × 128 matrix, 40 × 40 mm<sup>2</sup> FOV; 2-mm slice thickness]

was used to acquire seven slices in each imaging plane (axial, coronal, sagittal) for proper positioning of subsequent scans. A multislice T<sub>2</sub>-weighted fast-spin echo scan with eight echoes and 8.0 ms echo spacing (effective echo time of 32 ms) was then collected with TR = 2000 ms, 32 × 32 mm<sup>2</sup> FOV, 128 × 128 matrix, number of acquisitions = 16, and eight coronal slices of 2 mm thickness.

### PET/CT Imaging

PET/CT imaging was performed within 24 h of MR imaging in rats with confirmed tumors (n=14). Tumor-bearing rats were administered 130 – 200 MBq/0.2 mL [<sup>18</sup>F]DPA-714 *via* a jugular catheter while in a microPET Focus 220 (Siemens). Data were collected in list-mode format for 90 minutes, followed by a CT (microCAT II, Siemens) for attenuation correction. For displacement studies (n=4), DPA-714 (10 mg/kg) was injected at 30 min *via* jugular catheter.

The dynamic PET acquisition was divided into twelve, ten-second frames for the first two minutes, three, sixty-second frames for the following three minutes, followed by seventeen, three-hundred second frames for the duration of the scan. The raw data within each frame was then binned into 3D sinograms with a span of three and ring difference of 47. The sinograms were reconstructed into tomographic images (128 × 128 × 95) with voxel sizes of 0.095 × 0.095 × 0.08 cm<sup>3</sup>, after applying scatter and attenuation corrections, using an ordered-subsets expectation-maximization (OS-EM 2D) algorithm with 16 subsets and four iterations. Attenuation correction was accomplished by generating an attenuation map from the CT image. The CT image was first co-registered with the microPET image, segmented, and then projected into sinogram space with a span of 47 and ring difference of 23.

### Measurement of [<sup>18</sup>F]DPA-714 in Plasma

Immediately following administration of [<sup>18</sup>F]DPA-714, arterial blood samples (50 μL) were collected at 10-s intervals during the first minute of scanning, followed by collection at 90 s, and 2, 8, 12, 20, 30, 45, 60, 75, and 90 min. Blood samples (50 μL) were centrifuged at 14,000 RPM for 5 min in a microcentrifuge. The plasma (15 μL) was then removed and the radioactivity measured in a NaI well counter (Capintec).

### HPLC Radiometabolite Analysis

Briefly, arterial blood (200 μL) was collected at 2, 12, 30, 60, and 90 min. Following centrifugation, plasma was extracted with acetonitrile:water (340 mL, 7:1, v/v). The mixture was centrifuged and the supernatant used for reversed-phase HPLC analysis using 0.1 M aqueous ammonium acetate (NH<sub>4</sub>)OAc (pH 10) and acetonitrile (30:70; v/v) at 1.0 mL/min on a C18 Dynamax 250 × 4.6 mm (Varian) column. Radiochromatographic data were recorded and collected using a radioisotope detector (Bioscan), decay-corrected to time zero of each radiochromatogram, and smoothed using a locally weighted scatter plot smoothing method(26). The plasma time-activity curve was corrected according to the fraction of unchanged radioligand.

### Histology

Whole brains were harvested and fixed in 4% formalin for 48 h, followed by paraffin embedding for immunohistochemistry (IHC). Tissue sections of 5.0-μm thickness were taken and TSPO immunoreactivity assessed using a TSPO-specific rabbit polyclonal antibody, a gift from Professor V. Papadopoulos of McGill University, Montreal, Canada. Immunoreactivity was assessed using an HRP Detection Kit (Dako). Hematoxylin and eosin (H&E) staining was used to quantify cell density and tumor localization. For histology quantification, optical density measurements of multi-spectral image cubes were collected

using a CRI Nuance camera and the total intensity of positive pixels was determined as reported previously(22).

### Image Analysis and Modeling

Time-activity curves (TACs) were generated by manually drawing three-dimensional volumes of interest over tumor and contralateral brain using ASIPro (Siemens). The arterial input function (AIF) was computed from plasma sampling during imaging and corrected for metabolism of the parent ligand. Of the fourteen animals imaged in this study, data collected from three animals were excluded from modeling due to insufficient collection of arterial blood required for AIF determination. Both a 2-compartment, 2-rate constant kinetic model and a 3-compartment, 4-rate constant kinetic model were used to characterize [<sup>18</sup>F]DPA-714 pharmacokinetics with COMKAT software package. Model fit was determined by inspection. In the 2-compartment, 2-rate constant kinetic model, we determined model parameters for the influx ( $K_1$ ) and efflux ( $k_2$ ) rate constants of the radioligand diffusion between the plasma and tissue compartments. In the 3-compartment, 4-rate constant kinetic model, we determined model parameters for influx ( $K_1$ ) and efflux ( $k_2$ ) and exchange constants between specific binding ( $k_3$ ) and free ligand (including non-specific binding) ( $k_4$ ) compartments for both normal brain tissue and tumor. For the 3-compartment, 4-rate constant kinetic model, the total volume of distribution ( $V_T$ ) was then calculated using the equation  $V_T = (K_1/k_2)(1+k_3/k_4)$  for the whole brain (excluding tumor) and for the tumor(27). Additionally, using the first 60 minutes of data (beyond which, tracer was undetectable in blood), a graphical analysis method(28) was used to estimate the total distribution volume for the whole brain (excluding tumor) and tumor. Analysis of statistical significance utilized the Student's T-test (Prism 4.0).

## RESULTS

### Specific Binding of DPA-714 to TSPO in C6 Glioma Cell Line Homogenates

Previous studies explored [<sup>18</sup>F]DPA-714 within the context of neuroinflammation(25, 29). Our interest in assaying TSPO expression in glioma led us to evaluate the specific binding of DPA-714 in glioma cell line homogenates (Fig. 1). We found DPA-714 to be highly specific for TSPO, exhibiting robust dose-dependent displacement of the isoquinoline carboxamide [<sup>3</sup>H]PK 11195 to near-background levels. Non-linear regression analysis of the binding data yielded an IC<sub>50</sub> for DPA-714 of approximately 10.9 nM, similar to our previous observations with the aryloxyanilide PBR06(22).

### In Vivo Uptake of [<sup>18</sup>F]DPA-714 in C6 Glioma

Prior to PET imaging with [<sup>18</sup>F]DPA-714, brain tumors were localized using T<sub>2</sub>-weighted MRI. Similar to previous observations, C6 tumors exhibited marked hyperintensity indicative of longer T<sub>2</sub> relaxation times compared to surrounding brain (Fig. 2A). Dynamic PET imaging of [<sup>18</sup>F]DPA-714 illustrated that the majority of the uptake in the brain was localized to tumor tissue, with only modest accumulation in adjacent, normal areas of the brain (Fig. 2B, 2D). Over the last 30 minutes of the PET scan, total radioactivity levels in tumor tissue were approximately four-fold higher than normal brain. Over the course of imaging, a modest level of radioactivity localized to the skull, indicating defluorination that was later confirmed by HPLC radiometabolite analysis (Table 1, Supplemental Figure 1). Accumulation of [<sup>18</sup>F]DPA-714 was observed in the olfactory epithelium and Harderian glands (Supplemental Table 1), which had little impact on brain tumor imaging. Figure 2C illustrates a typical TAC for tumor, normal brain, and plasma activity for a typical 90 minute scan. We found that [<sup>18</sup>F]DPA-714 washed into both normal brain and tumor tissue rapidly, but washout from tumor tissue was much slower compared to normal brain. Following the initial spike in plasma activity consistent with tracer injection, [<sup>18</sup>F]DPA-714 rapidly cleared

the plasma. Imaging-matched brains were processed for staining and IHC. Using standard H&E staining to localize the tumor (Fig. 2E), we found that TSPO immunoreactivity was significantly higher in the tumor than in normal brain (Fig. 2F). Consistent with previous studies of TSPO expression in glioma, TSPO protein levels measured by IHC optical density were three- to four-fold higher in tumor relative to normal brain tissue (16, 22). Overall, we found excellent agreement between [<sup>18</sup>F]DPA-714 accumulation and TSPO protein levels as measured by IHC.

### ***In vivo* Displacement of [<sup>18</sup>F]DPA-714**

To evaluate the *in vivo* TSPO specificity of [<sup>18</sup>F]DPA-714, we carried out displacement studies in C6-bearing rats using DPA-714. During the dynamic PET study, excess (10 mg/kg) DPA-714 was administered intravenously 30 minutes following injection of [<sup>18</sup>F]DPA-714. Summation of the first 30 minutes of the PET scan prior to injection of DPA-714 (0 – 30 min) demonstrated typical uptake characteristics of [<sup>18</sup>F]DPA-714 (Fig. 3A). However, summation of the final 30 minutes of the PET scan (60 – 90 min) demonstrated significant displacement of [<sup>18</sup>F]DPA-714 in normal brain and tumor tissue (Fig. 3B). Accordingly, TAC analysis (Fig. 3C) demonstrated that following injection of DPA-714, tumor activity was reduced approximately 75% compared to the peak tumor uptake in the animal shown. Over multiple animals with comparatively larger and smaller tumors (n = 4), we observed a mean displacement of peak uptake of greater than 60%. Interestingly, in heterogeneous tumors featuring central necrosis, tracer uptake and specificity appeared greatest in actively proliferating tumor regions. Furthermore, minor, non-displaceable pooling of [<sup>18</sup>F]DPA-714 was observed in regions of central necrosis, although levels pooling in these regions tended to be reduced or similar to uptake associated normal, healthy brain.

### **Direct Comparison of [<sup>18</sup>F]DPA-714 and [<sup>18</sup>F]PBR06**

To further evaluate the *in vivo* performance of [<sup>18</sup>F]DPA-714 in tumor studies, we directly compared the localization and relative tissue uptake of this tracer in C6 glioma-bearing cohorts (n=2) to an aryloxyanilide TSPO PET ligand [<sup>18</sup>F]PBR06. A representative study is shown in Fig. 4. Tumors were initially localized with T<sub>2</sub>-weighted MRI (Fig. 4A). Subsequently, serial dynamic PET imaging studies utilizing [<sup>18</sup>F]PBR06 (Fig. 4B) or [<sup>18</sup>F]DPA-714 (Fig. 4C) were carried out approximately 24 hours apart. As shown in Fig. 4, both tracers exhibited similar localization to tumor tissue, with only modest retention in the normal brain. Both tracers exhibited similar rapid clearance from plasma and normal brain. However, TAC analysis illustrated that [<sup>18</sup>F]DPA-714 was retained in tumor tissue to a somewhat greater extent than [<sup>18</sup>F]PBR06, which manifested as a modestly higher signal-to-noise ratio (tumor/normal) for [<sup>18</sup>F]DPA-714 over the last 30 minutes of the PET scan.

### **Characterization of [<sup>18</sup>F]DPA-714 Radiometabolites**

Detectable [<sup>18</sup>F]DPA-714 radiometabolites included free [<sup>18</sup>F]fluoride (retention time 2.5 min) and a single radiometabolite more hydrophilic than DPA-714 (retention time, 4.0 min; parent tracer retention time, 5.0 min). As shown in Table 1, immediately following intravenous injection of [<sup>18</sup>F]DPA-714, the parent tracer accounted for approximately 95% of the whole plasma radioactivity. Subsequently, we observed a steady decrease of parent ligand in the plasma that was roughly equivalent to the increase in free <sup>18</sup>F-fluoride over the course of a given imaging study (Supplemental Figure 1), suggesting the primary metabolism observed in these studies was defluorination. Levels of the observed hydrophilic radiometabolite were relatively constant beyond the first 10 minutes of the scan, suggesting that appearance of this species was offset by further metabolism and/or subsequent clearance.

## Compartmental Modeling

To describe the pharmacokinetics of [<sup>18</sup>F]DPA-714, we evaluated 2-compartment, 2-kinetic parameter and 3-compartment, 4-kinetic parameter models. As determined by inspection, fit of the [<sup>18</sup>F]DPA-714 PET data was superior in the 3-compartment, 4-kinetic parameter model and the 2-compartment model was not considered further (Fig. 5A and 5B). Utilizing the 3-compartment, 4-kinetic parameter model and the metabolite-corrected AIF,  $K_1/k_2$  and  $k_3/k_4$  were determined for tumor tissue and normal brain (Table 2). Compared with normal brain, tumor tissues tended to exhibit a higher  $K_1/k_2$  and  $k_3/k_4$ . Estimation of  $V_T$  derived from kinetic parameters and graphical estimation (Fig. 6) was performed both in brain and tumor. Ratios of  $V_T$  and %ID/cc between tumor and brain obtained from both methods of estimation were highly similar and yielded statistically significant values that closely mirrored TSPO expression as measured by immunohistochemistry (Table 2).

## DISCUSSION

A considerable body of research suggests that TSPO can serve as an important biomarker in oncology. Numerous preclinical and clinical studies have demonstrated prognostic implications associated with elevated TSPO expression in multiple tumor types, including the breast(7, 8), prostate(9), oral cavity(10), colon(11–13), liver(14), and brain(15, 16). The first evidence supporting the hypothesis that TSPO ligands could be used for detection and grading of human brain tumors emerged more than twenty years ago(16, 30, 31), where autoradiographical (<sup>3</sup>H]PK 11195) and PET ([<sup>11</sup>C]PK 11195) studies evaluated TSPO expression in experimental models of glioma, post-mortem human brain sections(15, 16, 30, 32) and patients with glioma(33). While these early studies established the potential utility of TSPO ligands for brain tumor imaging, the most prominent TSPO-selective ligand available at the time, PK 11195, suffered from relatively modest *in vivo* uptake and attendant contrast in tumor tissue compared to normal brain. Furthermore, PK 11195 previously demonstrated considerable levels of non-displaceable ligand binding *in vivo*(33). Both of these conditions led to ligand uptake that marginally reflected actual TSPO expression levels. These issues recently led us to explore novel TSPO ligands with potentially improved pharmacokinetic properties and *in vivo* specificity in cancer imaging studies.

For example, we recently reported the first preclinical utilization of an aryloxyanilide-based TSPO ligand, [<sup>18</sup>F]PBR06, for quantitative assessment of TSPO expression in glioma(22). These studies demonstrated that [<sup>18</sup>F]PBR06 is a highly promising tracer for visualization of brain tumors, as well as quantification of TSPO expression in tumor and surrounding normal tissue. Compared with previous reports using [<sup>11</sup>C]PK 11195 in brain tumors, [<sup>18</sup>F]PBR06 demonstrated superior TSPO specificity *in vivo*, resulting in close agreement between tracer accumulation and TSPO protein levels.

In this study, we evaluated the pyrazolopyrimidine [<sup>18</sup>F]DPA-714 in analogous preclinical studies. Like [<sup>18</sup>F]PBR06, [<sup>18</sup>F]DPA-714 exhibited uptake that closely mirrored TSPO expression in tumor and normal tissues. Indeed, both tracers exhibited similar accumulation and clearance when compared in the same glioma-bearing animals. Furthermore, [<sup>18</sup>F]DPA-714 was highly displaceable from normal and tumor tissues. We observed a modest degree of non-displaceable pooling of [<sup>18</sup>F]DPA-714 in regions of the tumor that appeared to correlate with central necrosis, although uptake in necrosis was significantly lower than that observed in actively growing portions of the tumor. Analogous to our studies with [<sup>18</sup>F]PBR06, [<sup>18</sup>F]DPA-714 time-activity curves derived from tumor and normal brain could be fit to a 3-compartment, 4-kinetic parameter compartmental model, enabling tracer quantitation (e.g.  $V_T$ ) in tumor tissue and normal brain. In general, TACs for [<sup>18</sup>F]DPA-714 uptake in both tumor and normal tissue were remarkably consistent across numerous

animals (Supplemental Figure 2), suggesting the robustness and reproducibility of this imaging approach. Though the aryloxyanilide [<sup>18</sup>F]PBR06 and pyrazolopyrimidine [<sup>18</sup>F]DPA-714 both appear to be promising tracers in this preclinical setting, further studies to better characterize determinants such as *in vivo* metabolism and tissue pharmacodynamics will likely reveal important differences between these two unique scaffolds. We envision that evaluation of these and similar agents within the context of other solid tumors such as colorectal(11–13) and breast(7, 8) cancer may shed further light upon the rational selection of TSPO ligands for cancer imaging.

## CONCLUSION

These preclinical studies illustrate the feasibility of using [<sup>18</sup>F]DPA-714 for visualization of TSPO-expressing brain tumors. Importantly, [<sup>18</sup>F]DPA-714 appears suitable for quantitative assay of tumor TSPO levels *in vivo*. Given the relationship between elevated TSPO levels and poor outcome in oncology, these studies suggest the potential of [<sup>18</sup>F]DPA-714 PET to serve as a novel predictive cancer imaging modality.

## Supplementary Material

Refer to Web version on PubMed Central for supplementary material.

## Acknowledgments

This work was supported by funding from the National Cancer Institute (1R01 CA140628; K25 CA127349; 1RC1 CA145138; 1P50 CA128323; U24 CA126588) and training grants (5R25 CA092043-09; T32 EB003817; R25 CA136440). The authors gratefully acknowledge Professor Vassilios Papadopoulos of McGill University for the TSPO antibody. Clare A. Osborne, Zou Yue, and Fuxue Xin provided imaging support.

## REFERENCES

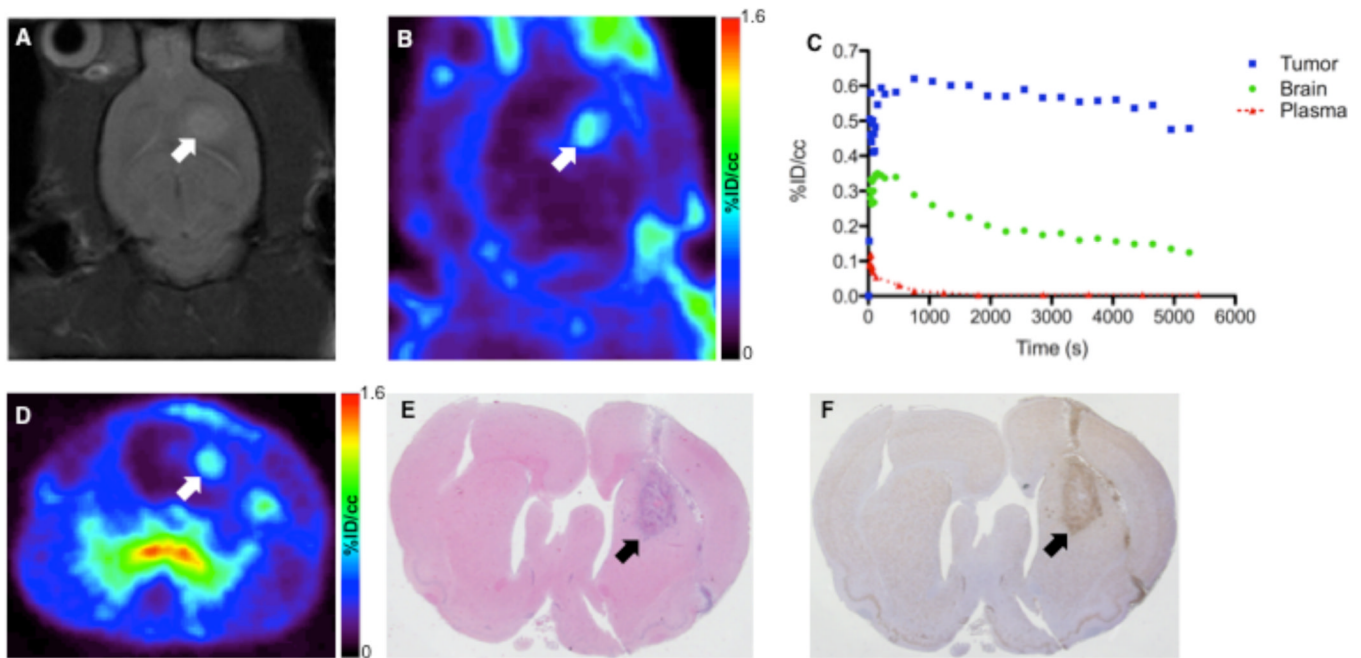
1. Dhermain FG, Hau P, Lanfermann H, Jacobs AH, van den Bent MJ. Advanced MRI and PET imaging for assessment of treatment response in patients with gliomas. *Lancet Neurol*. 2010; 9:906–920. [PubMed: 20705518]
2. van den Bent MJ, Vogelbaum MA, Wen PY, Macdonald DR, Chang SM. End point assessment in gliomas: novel treatments limit usefulness of classical Macdonald's Criteria. *J Clin Oncol*. 2009; 27:2905–2908. [PubMed: 19451418]
3. Papadopoulos V, Baraldi M, Guilarte TR, et al. Translocator protein (18kDa): new nomenclature for the peripheral-type benzodiazepine receptor based on its structure and molecular function. *Trends Pharmacol Sci*. 2006; 27:402–409. [PubMed: 16822554]
4. Papadopoulos V, Lecanu L. Translocator protein (18 kDa) TSPO: an emerging therapeutic target in neurotrauma. *Exp Neurol*. 2009; 219:53–57. [PubMed: 19409385]
5. Diorio D, Welner SA, Butterworth RF, Meaney MJ, Suranyi-Cadotte BE. Peripheral benzodiazepine binding sites in Alzheimer's disease frontal and temporal cortex. *Neurobiol Aging*. 1991; 12:255–258. [PubMed: 1652108]
6. Messmer K, Reynolds GP. Increased peripheral benzodiazepine binding sites in the brain of patients with Huntington's disease. *Neurosci Lett*. 1998; 241:53–56. [PubMed: 9502214]
7. Hardwick M, Fertikh D, Culty M, Li H, Vidic B, Papadopoulos V. Peripheral-type benzodiazepine receptor (PBR) in human breast cancer: correlation of breast cancer cell aggressive phenotype with PBR expression, nuclear localization, and PBR-mediated cell proliferation and nuclear transport of cholesterol. *Cancer Res*. 1999; 59:831–842. [PubMed: 10029072]
8. Carmel I, Fares FA, Leschiner S, Scherubl H, Weisinger G, Gavish M. Peripheral-type benzodiazepine receptors in the regulation of proliferation of MCF-7 human breast carcinoma cell line. *Biochem Pharmacol*. 1999; 58:273–278. [PubMed: 10423168]



9. Fafalios A, Akhavan A, Parwani AV, Bies RR, McHugh KJ, Pflug BR. Translocator protein blockade reduces prostate tumor growth. *Clin Cancer Res.* 2009; 15:6177–6184. [PubMed: 19789311]
10. Nagler R, Ben-Izhak O, Savulescu D, et al. Oral cancer, cigarette smoke and mitochondrial 18kDa translocator protein (TSPO) - In vitro, in vivo, salivary analysis. *Biochim Biophys Acta.* 2010; 1802:454–461. [PubMed: 20085808]
11. Maaser K, Grabowski P, Sutter AP, et al. Overexpression of the peripheral benzodiazepine receptor is a relevant prognostic factor in stage III colorectal cancer. *Clin Cancer Res.* 2002; 8:3205–3209. [PubMed: 12374690]
12. Deane NG, Manning HC, Foutch AC, et al. Targeted imaging of colonic tumors in smad3<sup>-/-</sup> mice discriminates cancer and inflammation. *Mol Cancer Res.* 2007; 5:341–349. [PubMed: 17426249]
13. Maaser K, Hopfner M, Jansen A, et al. Specific ligands of the peripheral benzodiazepine receptor induce apoptosis and cell cycle arrest in human colorectal cancer cells. *Br J Cancer.* 2001; 85:1771–1780. [PubMed: 11742501]
14. Venturini I, Zeneroli ML, Corsi L, et al. Up-regulation of peripheral benzodiazepine receptor system in hepatocellular carcinoma. *Life Sci.* 1998; 63:1269–1280. [PubMed: 9771915]
15. Black KL, Ikezaki K, Toga AW. Imaging of brain tumors using peripheral benzodiazepine receptor ligands. *J Neurosurg.* 1989; 71:113–118. [PubMed: 2544689]
16. Starosta-Rubinstein S, Ciliax BJ, Penney JB, McKeever P, Young AB. Imaging of a glioma using peripheral benzodiazepine receptor ligands. *Proc Natl Acad Sci U S A.* 1987; 84:891–895. [PubMed: 3027710]
17. Nagler R, Savulescu D, Krayzler E, Leschiner S, Veenman L, Gavish M. Cigarette smoke decreases salivary 18 kDa translocator protein binding affinity - in association with oxidative stress. *Curr Med Chem.* 2010; 17:2539–2546. [PubMed: 20491643]
18. Galieue S, Casellas P, Kramar A, Tinel N, Simony-Lafontaine J. Immunohistochemical assessment of the peripheral benzodiazepine receptor in breast cancer and its relationship with survival. *Clin Cancer Res.* 2004; 10:2058–2064. [PubMed: 15041726]
19. Miettinen H, Kononen J, Haapasalo H, et al. Expression of peripheral-type benzodiazepine receptor and diazepam binding inhibitor in human astrocytomas: relationship to cell proliferation. *Cancer Res.* 1995; 55:2691–2695. [PubMed: 7780986]
20. Hardwick M, Rone J, Han Z, Haddad B, Papadopoulos V. Peripheral-type benzodiazepine receptor levels correlate with the ability of human breast cancer MDA-MB-231 cell line to grow in SCID mice. *Int J Cancer.* 2001; 94:322–327. [PubMed: 11745409]
21. Dolle F, Luus C, Reynolds A, Kassiou M. Radiolabelled molecules for imaging the translocator protein (18 kDa) using positron emission tomography. *Curr Med Chem.* 2009; 16:2899–2923. [PubMed: 19689272]
22. Buck JR, McKinley ET, Hight MR, et al. Quantitative, preclinical PET of translocator protein expression in glioma using 18F-N-fluoroacetyl-N-(2,5-dimethoxybenzyl)-2-phenoxyaniline. *J Nucl Med.* 2011; 52:107–114. [PubMed: 21149488]
23. Tang D, Buck JR, Hight MR, Manning HC. Microwave-assisted organic synthesis of a high-affinity pyrazolo-pyrimidinyl TSPO ligand. *Tetrahedron Lett.* 2010; 51:4595–4598. [PubMed: 20689673]
24. Kozikowski AP, Kotoula M, Ma D, Boujrad N, Tuckmantel W, Papadopoulos V. Synthesis and biology of a 7-nitro-2,1,3-benzoxadiazol-4-yl derivative of 2-phenylindole-3-acetamide: a fluorescent probe for the peripheral-type benzodiazepine receptor. *J Med Chem.* 1997; 40:2435–2439. [PubMed: 9258348]
25. Chauveau F, Van Camp N, Dolle F, et al. Comparative evaluation of the translocator protein radioligands 11C-DPA-713, 18F-DPA-714, and 11C-PK11195 in a rat model of acute neuroinflammation. *J Nucl Med.* 2009; 50:468–476. [PubMed: 19223401]
26. Cleveland WS, Devlin SJ. Locally weighted regression - an approach to regression-analysis by local fitting. *Journal of the American Statistical Association.* 1988; 83:596–610.
27. Innis RB, Cunningham VJ, Delforge J, et al. Consensus nomenclature for in vivo imaging of reversibly binding radioligands. *J Cereb Blood Flow Metab.* 2007; 27:1533–1539. [PubMed: 17519979]

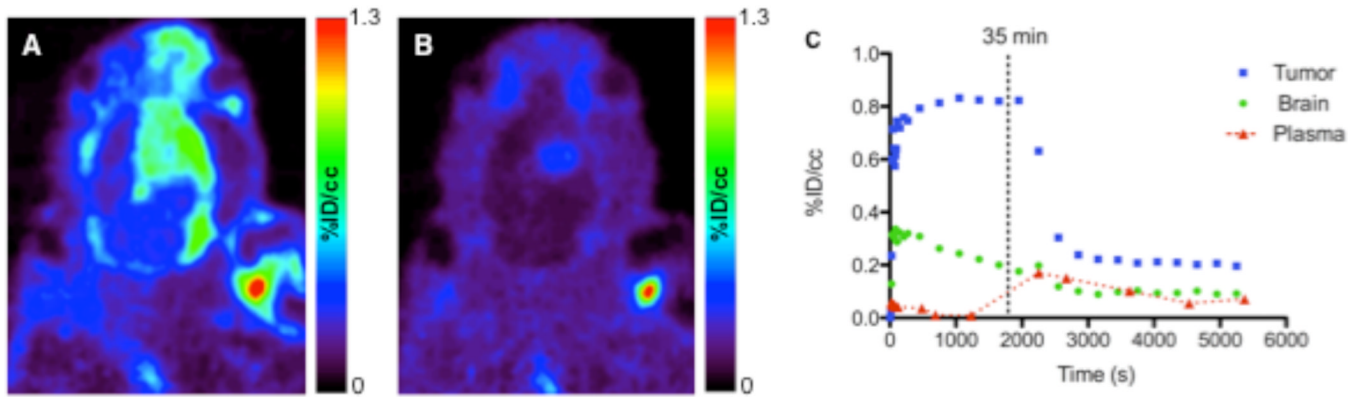
28. Logan J, Fowler JS, Volkow ND, Wang GJ, Ding YS, Alexoff DL. Distribution volume ratios without blood sampling from graphical analysis of PET data. *J Cereb Blood Flow Metab.* 1996; 16:834–840. [PubMed: 8784228]
29. Martin A, Boisgard R, Theze B, et al. Evaluation of the PBR/TSPO radioligand [(18F)DPA-714 in a rat model of focal cerebral ischemia. *J Cereb Blood Flow Metab.* 2010; 30:230–241. [PubMed: 19794397]
30. Olson JM, Junck L, Young AB, Penney JB, Mancini WR. Isoquinoline and peripheral-type benzodiazepine binding in gliomas: implications for diagnostic imaging. *Cancer Res.* 1988; 48:5837–5841. [PubMed: 3262414]
31. Cornu P, Benavides J, Scatton B, Hauw JJ, Philippon J. Increase in omega 3 (peripheral-type benzodiazepine) binding site densities in different types of human brain tumours. A quantitative autoradiography study. *Acta Neurochir (Wien).* 1992; 119:146–152. [PubMed: 1336303]
32. Junck L, Olson JM, Ciliax BJ, et al. PET imaging of human gliomas with ligands for the peripheral benzodiazepine binding site. *Ann Neurol.* 1989; 26:752–758. [PubMed: 2557794]
33. Pappata S, Cornu P, Samson Y, et al. PET study of carbon-11-PK 11195 binding to peripheral type benzodiazepine sites in glioblastoma: a case report. *J Nucl Med.* 1991; 32:1608–1610. [PubMed: 1651383]





**FIGURE 2.**

(A) T<sub>2</sub>-weighted MR image of C6 glioma-bearing rat in right hemisphere. (B) Transverse PET image obtained from dynamic scan of [<sup>18</sup>F]DPA-714 PET (summed dynamic scan, 0–90 min). (C) [<sup>18</sup>F]DPA-714 time–activity curves for tumor (blue), contralateral brain (green), and plasma (red). (D) Coronal PET image obtained from dynamic scan of [<sup>18</sup>F]DPA-714 PET (summed dynamic scan, 0–90 min). (E) Standard hematoxylin and eosin staining of serial tissue section. (F) Immunohistochemistry analysis of TSPO expression in typical C6 glioma. Tumor location is indicated with arrows in the images.

**FIGURE 3.**

*In vivo* displacement of [ $^{18}\text{F}$ ]DPA-714 in C6 glioma-bearing rat. Relative [ $^{18}\text{F}$ ]DPA-714 uptake before (A) and after (B) intravenous infusion of excess DPA-714. (C) [ $^{18}\text{F}$ ]DPA-714 time-activity curves generated for tumor (blue), contralateral brain (green), and plasma (red).

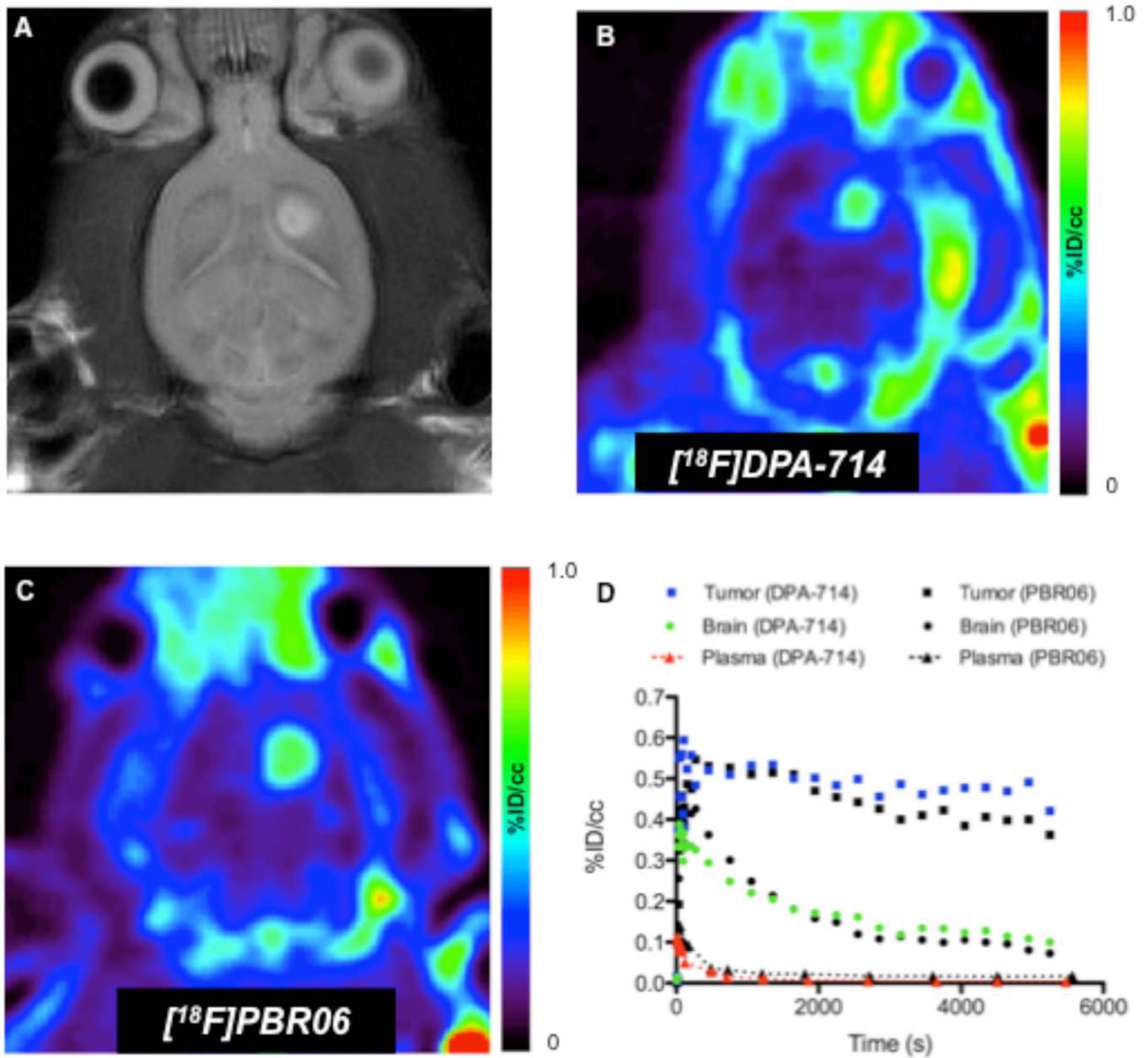


**FIGURE 4.**

Comparison of  $[^{18}\text{F}]\text{PBR06}$  and  $[^{18}\text{F}]\text{DPA-714}$  in the same glioma-bearing rat. (A) T<sub>2</sub>-weighted MR image of rat bearing C6 glioma in right hemisphere. (B)  $[^{18}\text{F}]\text{PBR06}$  PET image (summed dynamic scan over the last 30 min). (C)  $[^{18}\text{F}]\text{DPA-714}$  PET image (summed dynamic scan over the last 30 min). (D)  $[^{18}\text{F}]\text{DPA-714}$  time-activity curves generated for tumor (blue), contralateral brain (green), and plasma (red). For comparison,  $[^{18}\text{F}]\text{PBR06}$  time-activity curves are shown in black.

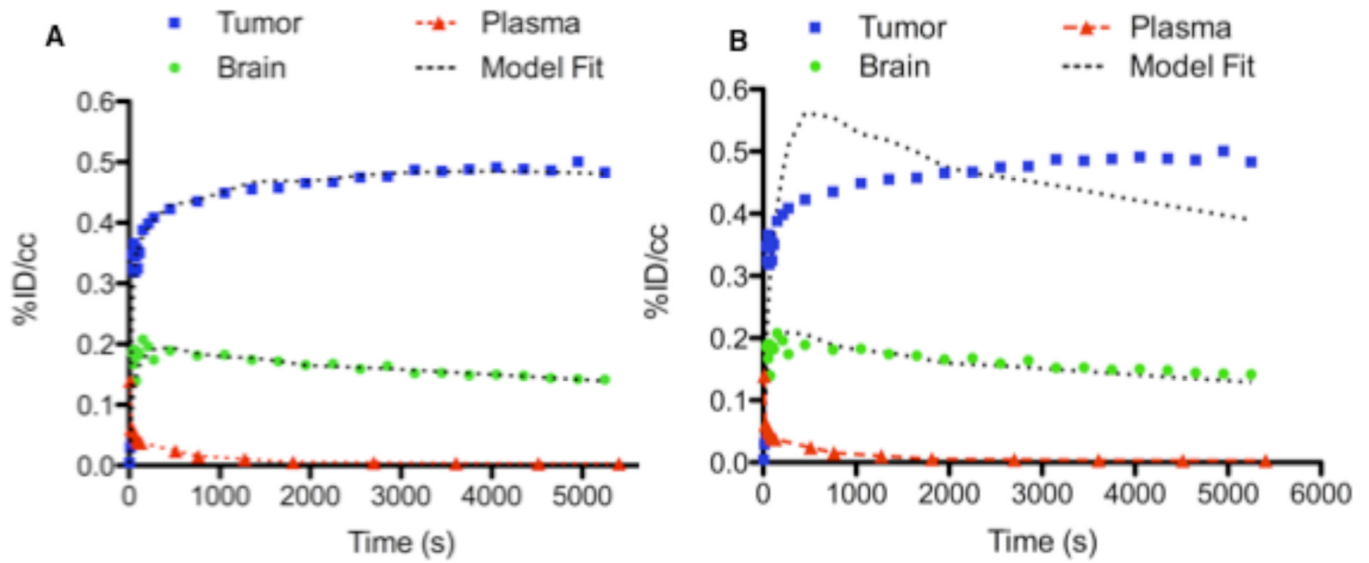


**FIGURE 5.** Pharmacokinetic model fit of typical [ $^{18}\text{F}$ ]DPA-714 time-activity curves to 2-compartment, 2-kinetic parameter (A) and 3-compartment, 4-kinetic parameter models (B). Time-activity curves for tumor (blue), contralateral brain (green), and plasma (red) are shown with the associated model fit.

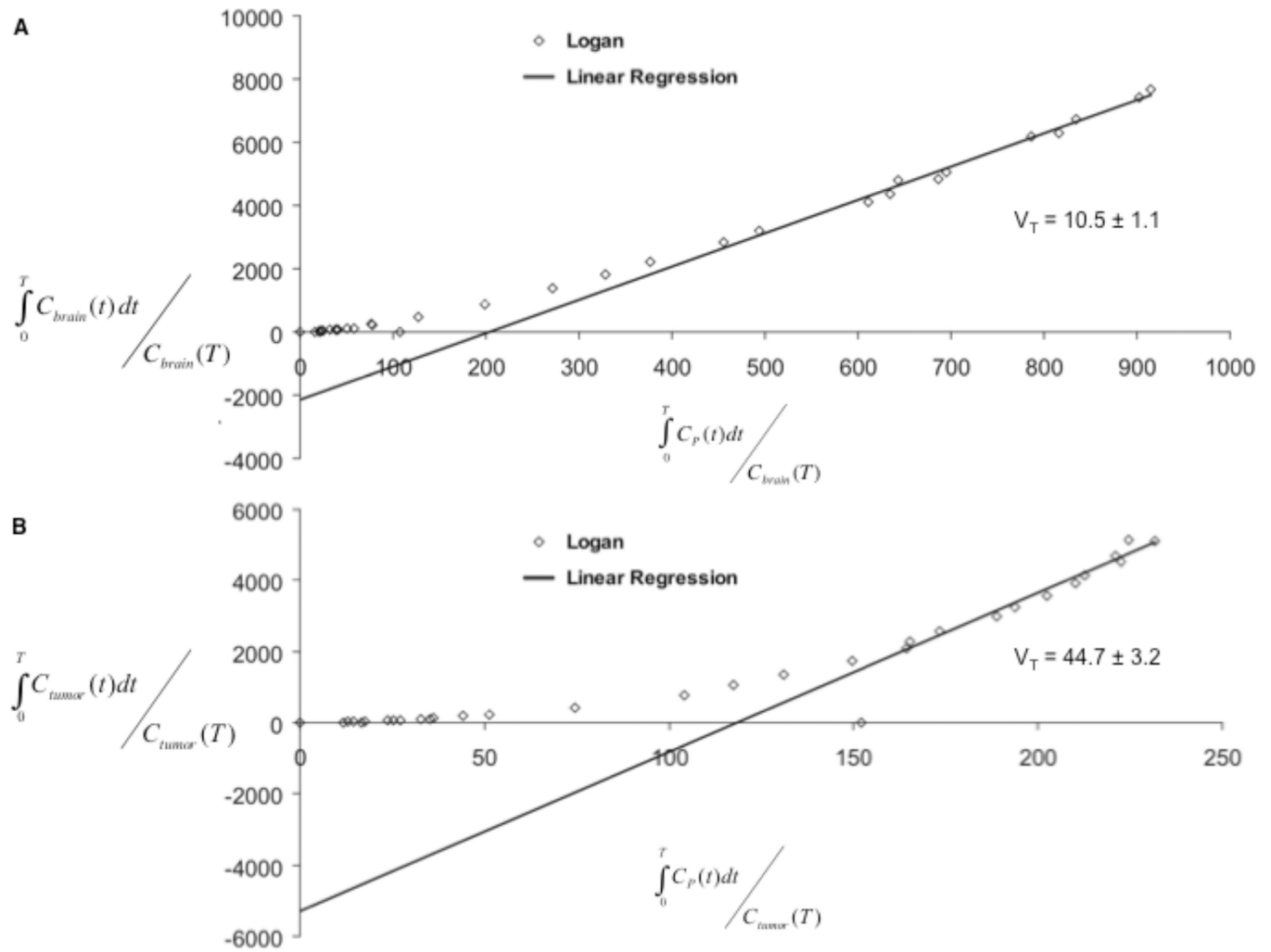


**FIGURE 6.** Representative graphical analysis of  $V_T$  for a subject from this investigation. The fit was carried out for normal brain (A) and for tumor (B). Solid grey line = Linear Regression; start time for linear regression, “t\*”.



**TABLE 1**HPLC Radiometabolite Analysis of [<sup>18</sup>F]DPA-714 (*mean ± SD*).

<b>P.I. Time</b>	<b>% [<sup>18</sup>F]DPA-714</b>	<b>%<sup>18</sup>F<sup>-</sup></b>	<b>% Metabolite</b>
2 (N=7)	95 ± 6.0	2 ± 3.3	3 ± 3.7
12 (N=7)	68 ± 7.4	13 ± 6.7	19 ± 5.8
30 (N=7)	44 ± 8.9	37 ± 5.4	19 ± 8.8
60 (N=7)	27 ± 6.2	50 ± 15.0	23 ± 7.3
90 (N=5)	22 ± 17.8	64 ± 12.1	14 ± 3.8

TABLE 2

Parameter Estimations for [<sup>18</sup>F]DPA-714 Uptake (*mean* ± *SEM*).

	$K_1/k_2$ (mL/g)	$k_3/k_4$	$V_T$ (mL/g) <sup>†</sup>	$V_T$ (mL/g) <sup>‡</sup>	%ID/cc
Tumor (N=11)	6.867 ± 1.226	8.913 ± 1.155	70.033 ± 14.729	57.440 ± 11.742	0.088 ± 0.011
Brain (N=11)	3.619 ± 0.551	4.024 ± 0.842	15.963 ± 3.566	14.570 ± 2.823	0.331 ± 0.036
P-value	0.0762	0.0021	0.0017	0.0029	<0.0001

<sup>†</sup>From kinetic parameters.

<sup>‡</sup>From graphical analysis.